Calibration-quality adiabatic potential energy surfaces for H3+ and its isotopologues

Michele Pavanello, Ludwik Adamowicz, Alexander Alijah, Nikolai F. Zobov, Irina I. Mizus et al.

Additional information on J. Chem. Phys.
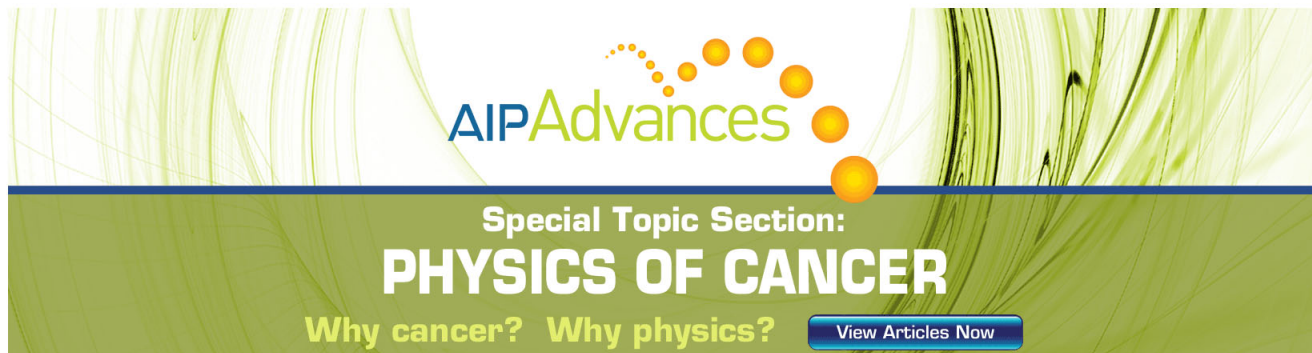
Calibration-quality adiabatic potential energy surfaces for H_3^+ and its isotopologues

Michele Pavanello,[1,a)] Ludwik Adamowicz,[2,b)] Alexander Alijah,[3,c)] Nikolai F. Zobov,[4] Irina I. Mizus,[4] Oleg L. Polyansky,[4,d)] Jonathan Tennyson,[5,e)] Tamás Szidarovszky,[6] and Attila G. Császár[6,f)]

[1]*Gorlaeus Laboratories, Leiden Institute of Chemistry, Leiden University, P.O. Box 9502, 2300 RA Leiden, The Netherlands*
[2]*Department of Chemistry, University of Arizona, Tucson, Arizona 85721, USA*
[3]*Groupe de Spectrométrie Moléculaire et Atmosphérique, GSMA, UMR CNRS 7331, Université de Reims Champagne-Ardenne, France*
[4]*Institute of Applied Physics, Russian Academy of Science, Ulyanov Street 46, Nizhnii Novgorod 603950, Russia*
[5]*Department of Physics and Astronomy, University College London, Gower Street, London WC1E 6BT, United Kingdom*
[6]*Laboratory of Molecular Structure and Dynamics, Institute of Chemistry, Eötvös University, H-1518 Budapest 112, P.O. Box 32, Hungary*

Calibration-quality *ab initio* adiabatic potential energy surfaces (PES) have been determined for all isotopologues of the molecular ion H_3^+. The underlying Born–Oppenheimer electronic structure computations used optimized explicitly correlated shifted Gaussian functions. The surfaces include diagonal Born–Oppenheimer corrections computed from the accurate electronic wave functions. A fit to the 41 655 *ab initio* points is presented which gives a standard deviation better than 0.1 cm^{-1} when restricted to the points up to 6000 cm^{-1} above the first dissociation asymptote. Nuclear motion calculations utilizing this PES, called GLH3P, and an exact kinetic energy operator given in orthogonal internal coordinates are presented. The ro-vibrational transition frequencies for H_3^+, H_2D^+, and HD_2^+ are compared with high resolution measurements. The most sophisticated and complete procedure employed to compute ro-vibrational energy levels, which makes explicit allowance for the inclusion of non-adiabatic effects, reproduces all the known ro-vibrational levels of the H_3^+ isotopologues considered to better than 0.2 cm^{-1}. This represents a significant (order-of-magnitude) improvement compared to previous studies of transitions in the visible. Careful treatment of linear geometries is important for high frequency transitions and leads to new assignments for some of the previously observed lines. Prospects for further investigations of non-adiabatic effects in the H_3^+ isotopologues are discussed. In short, the paper presents (a) an extremely accurate global potential energy surface of H_3^+ resulting from high accuracy *ab initio* computations and global fit, (b) very accurate nuclear motion calculations of all available experimental line data up to 16 000 cm^{-1}, and (c) results suggest that we can predict accurately the lines of H_3^+ towards dissociation and thus facilitate their experimental observation. © *2012 American Institute of Physics*. [http://dx.doi.org/10.1063/1.4711756]

I. INTRODUCTION

However simple the molecular ion H_3^+ may appear, it contains five quantum particles and thus the non-adiabatic treatment of its spectra within relativistic or even non-relativistic quantum mechanics is still not within reach. With the latest developments in the appropriate protocols and codes, variational non-adiabatic treatments of three-body systems within non-relativistic quantum mechanics are becoming commonplace. There are certain evolving techniques whereby four-particle systems, such as the isotopologues of the H_2 molecule, can be treated in a non-adiabatic and non-relativistic fashion. Larger systems can also be treated but only to a rather limited extent.[1]

When adiabatic quantum mechanical computations, based on the separation of nuclear and electronic degrees of freedom, are employed to determine the high-resolution spectra of small molecules, the following factors need to be investigated when the precision and the accuracy of the computed results is determined: (a) the electronic and nuclear Hamiltonians used for the computations; (b) the accuracy of the fundamental constants; (c) the accuracy and precision of the electronic energies computed over a grid; (d) the size and extent of the grid; (e) the number of electronic surfaces treated; (f) the accuracy of the fitting of the PES employing a suitable functional form and interpolating between the computed points;

a)Electronic mail: m.pavanello@chem.leidenuniv.nl.
b)Electronic mail: ludwik@u.arizona.edu.
c)Electronic mail: alexander.alijah@univ-reims.fr.
d)Electronic mail: oleg@theory.phys.ucl.ac.uk.
e)Electronic mail: j.tennyson@ucl.ac.uk.
f)Electronic mail: csaszar@chem.elte.hu.

(g) the choice of the masses in the nuclear motion computations; (h) the accuracy and precision of the variational nuclear motion treatment; and (i) the treatment of non-adiabatic effects.

The H_3^+ molecular ion has long been used as a benchmark system of quantum physical and quantum chemical interest; for example, a number of PESs have been computed for it using explicitly correlated electronic structure techniques.[2–5] The accuracy of these and other[6] PESs developed for the H_3^+ isotopologues can be tested against a multitude of high-resolution spectroscopy data available for the $H_{3-n}D_n^+$ system.[7–22] It turns out that even in the mid-infrared region ($n = 0$–3) *ab initio* transitions significantly more accurate than about 1 cm^{-1} can only be computed by treatment of non-Born–Oppenheimer effects. For transitions below 5 000 cm^{-1}, two of the authors developed an accurate *ab initio* model,[23] which reproduced the spectra of H_3^+ and its deuterated isotopologues to better than 0.1 cm^{-1} on average. However, a series of subsequent experimental studies on H_3^+,[9–12] H_2D^+, and D_2H^+ (Refs. 19–22) which extend the measurements to much higher frequencies have so far proved harder to model to high accuracy theoretically. These and other observations scattered in the literature suggest that there are significant remaining difficulties with non-Born–Oppenheimer effects.[21] Furthermore, particular care needs to be exercised with treatment of the system above the barrier to linearity.[11,24]

H_3^+ is a key astronomical species in the interstellar medium[25] and the atmospheres of gas giants[26,27] and has even been detected in supernova remnants.[28] Its spectroscopic detection in space relied on *ab initio* calculations[29] which have since helped to provide tabulations of key transitions,[30] extensive line lists,[31,32] partition functions,[33] and cooling functions.[34] There are aspects of these data which need improving: for example, the available cooling functions are not reliable at low temperatures which may be important for studies of primordial chemistry.[35]

Our aim is to generate adiabatic PESs with underlying *ab initio*, Born-Oppenheimer energies of an accuracy on the order of 10^{-8} E_h, which corresponds to sub 0.01 cm^{-1} and, for convenience, energies are largely given in cm^{-1} below. Such an accuracy level is not achievable with the use of any of the black-box electronic structure packages employing basis sets composed of one-electron functions. The need to move beyond the standard one-electron basis set approach has presented a long-standing challenge for electronic structure computations. In the past two decades several computational quantum chemistry groups responded to this challenge and became involved in a sort of "a race for the highest accuracy" for the H_3^+ molecular ion. The need for the high accuracy in the H_3^+ PES calculations is partially related to a higher accuracy one wants to achieve in the computational modeling of the ro-vibrational spectrum of the H_3^+ system. A more accurate and complete first-principles spectrum would allow for better assignment of the experimental spectrum, which is increasingly better measured and characterized. Ultimately, assignment of the Carrington bands[36] is the goal of computational studies of the rotational-vibrational spectra of H_3^+.

Among the milestones that have been particularly relevant for studies of the high-resolution spectrum of H_3^+ iso-

topologues one should mention the PES generated by Meyer *et al.*[6] (hereafter referred to as MBB) using the full configuration interaction method and, by modern standards, a fairly small basis set. The MBB PES includes 69 grid points with the energy reaching up to about 25 000 cm^{-1} above the bottom of the PES. The accuracy of the MBB PES was later improved by more precise computations performed with the CI method involving configuration functions multiplied by r_{12} pre-factors.[3] An even higher accuracy, claimed to be as high as 0.02 cm^{-1} at each point of the 69-point grid, was achieved by Cencek *et al.*[37] in their computations performed with explicitly correlated Gaussian functions, augmented with adiabatic and relativistic corrections. Recently, even further improved energies and more accurate calculations of the H_3^+ rovibrational spectrum were reported by Bachorz *et al.*[38] They produced total energies of H_3^+ with a claimed accuracy of 0.02 cm^{-1} at over 5000 PES points including many located above the barrier to linearity.

Even though significant progress has been made in the calculations of the H_3^+ ground-state PES, there is still considerable room for improvement, especially in the peripheral regions of the PES corresponding to dissociative geometrical configurations. Better electronic structure calculations need to involve longer, more accurate expansions of the wave function in terms of the basis functions and more effective optimization of their parameters. Such an improved optimization applied to the wave function expanded in terms of explicitly correlated shifted Gaussian functions (ECSGs) was recently developed and presented by the Adamowicz group.[5,39] In Ref. 39 the method was applied for the variational determination of the H_3^+ ground-state energy at its equilibrium structure (an equilateral triangle with a bond length of 1.65 bohr). It was shown that using up to 1000 Gaussians in the wave function expansion, the best variational energy upper bound ever for this system could be obtained. The best result of $-1.343\,835\,625\,02$ E_h exhibits an unprecedented precision of below 10^{-10} E_h. In Ref. 5, Pavanello *et al.* developed a procedure that allowed for the energy calculation to be carried out at multiple H_3^+ geometrical points, using for each point the wave function obtained for a nearby point with the Gaussian centers shifted in the direction of the shifted nuclei. With that procedure they recalculated the energies at all 69 MBB grid points and achieved the accuracy of 5×10^{-8} E_h (about 0.01 cm^{-1}), which is almost an order of magnitude improvement over the previous best literature computations.[37]

Recently, we have computed a new, ultra-high accuracy potential energy surface and used it to assign newly observed H_3^+ transitions in the mid-visible region of the spectrum.[13] In that study, the fully *ab initio* calculations presented reproduced the observed transition frequencies to within about 0.1 cm^{-1}. Here we give full details of this work, show that the model is equally applicable to the deuterated isotopologues of H_3^+, and present predicted vibrational band origins covering the entire visible region of the spectrum. Section II details the electronic structure calculations, Sec. III discusses our fitting to the *ab initio* grid points, and Sec. IV presents the results of our nuclear motion calculations. Possible future developments and our conclusions are discussed in Sec. V. Extensive data have been placed in the electronic archive[40] to aid those

interested in high accuracy spectroscopic and related studies on H_3^+ and its isotopologues.

II. ELECTRONIC STRUCTURE COMPUTATIONS

The adiabatic composite PESs of the H_3^+ isotopologues considered in this work were constructed by the addition of three independently generated surfaces: (a) the non-relativistic Born–Oppenheimer (BO) energy surface, (b) the diagonal Born–Oppenheimer correction (DBOC) surface, and (c) the relativistic correction (RC) surface. Generation of each of these surfaces is based on two steps, computation of the *ab initio* BO energies, DBOCs, and RCs on a grid of nuclear geometries, and subsequent fitting with properly chosen fit functions.

A. BO energies

The following two features distinguish our present H_3^+ PES computations from the ones published in the literature: (1) we calculate the BO energies of H_3^+ on a grid containing 41 655 nuclear geometries, the densest and most extended grid ever used in computations for the H_3^+ ion; and (2) the unprecedented high accuracy achieved in the BO energy calculation at every grid point.

Let us now explain in some detail the approach we use in the present study to determine BO energies for H_3^+. The spatial component of the variational wave function, $\Phi_M(\mathbf{r})$, of an n–electron system is expanded in terms of a set of M ECSGs, $\{g_k\}_{k=1,\dots M}$, as

$$\Phi_M(\mathbf{r}) = \sum_{k=1}^{M} C_k g_k(\mathbf{r}). \tag{1}$$

The ECSGs are the following functions:

$$g_k(\mathbf{r}) = \exp[-(\mathbf{r} - \mathbf{s}_k)'\overline{\mathbf{A}}_k(\mathbf{r} - \mathbf{s}_k)], \tag{2}$$

where $\mathbf{r}$ and $\mathbf{s}_k$ are $3n$ dimensional vectors of the electronic Cartesian coordinates and of the coordinates of the Gaussian shift, respectively, and the prime denotes the vector transposition. $\overline{\mathbf{A}}_k$ is a symmetric matrix of the Gaussian exponential coefficients defined as

$$\overline{\mathbf{A}}_k = \mathbf{A}_k \otimes \mathbf{I}_3, \tag{3}$$

with $\mathbf{I}_3$ being the 3×3 identity matrix and $\otimes$ denoting the Kronecker product. We represent the $\mathbf{A}_k$ matrix in the following Cholesky-factorized form: $\mathbf{A}_k = \mathbf{L}'_k\mathbf{L}_k$, where $\mathbf{L}_k$ is a lower triangular matrix. This factorization automatically assures that $\mathbf{A}_k$ is a positive definite matrix and $g_k(\mathbf{r})$ is a square-integrable function regardless of the particular choice of the $\mathbf{L}_k$ matrix elements. The $\mathbf{L}_k$ matrix together with the shift vector, $\mathbf{s}_k$, uniquely define the kth ECSG basis function, g_k.

In the calculation, the proper permutational symmetry needs to be implemented in the wave function so that it satisfies the Pauli exclusion principle. For the ground singlet state of H_3^+, the spatial wave function needs to be symmetric with respect to permutations of the coordinates of the two electrons which is achieved by adding to each g_k basis function (1) a

function with permuted coordinates of the shifts vector and permuted elements of the $\mathbf{A}_k$ matrix.

The total variational energy is calculated by solving the secular equation

$$\mathbf{HC} = \mathbf{SCE}, \tag{4}$$

where the elements of the Hamiltonian and overlap matrices, $\mathbf{H}$ and $\mathbf{S}$, are $H_{kl} = \langle g_k|\hat{H}|g_l\rangle$ and $S_{kl} = \langle g_k|g_l\rangle$, respectively. The diagonal matrix $\mathbf{E}$ comprises the BO energies of the ground and excited states. Those energies are functions of the nonlinear parameters of the ECSG basis functions, i.e., the $\mathbf{L}_k$ matrix elements and the elements of the $\mathbf{s}_k$ vectors.

Equation (4) is solved every time the nonlinear parameters are changed by the routine that runs the variational energy minimization. The optimization is carried out by the minimization of the energy functional with respect to the nonlinear parameters. For this purpose we use the truncated Newton minimum-search routine of Nash.[41] The input to the routine consists of three items: the values of the nonlinear parameters, the corresponding energy, and the energy gradient. In our calculations the gradient, which comprises the first derivatives of the energy with respect to the nonlinear parameters, is determined using the formulas obtained by analytical differentiation of the energy with respect to those parameters. The formulas involve the first derivative of the error function needed in the potential energy derivatives. The error-function derivative is obtained by numerical differentiation.[42]

The use of analytical energy gradients in the variational energy minimization sets our work apart from other works where the ECSG basis functions were utilized,[37,38] and where the gradient was approximated numerically. The efficiency of the optimization is significantly improved by the use of the analytical gradient. For instance, the best H_3^+ variational BO energy obtained with our gradient-based method[39] is two orders of magnitude more accurate than the one obtained with the procedure that involved the numerical derivatives.[43]

B. DBOCs

Beside the ECSG calculation of the total energy, other molecular properties have also been subjected to ECSG calculations. Properties, such as the transition dipole moments[44] and post-BO energy corrections,[45] have been computed. The calculations of molecular properties and post-BO energy corrections are often more sensitive to the shortcomings of Gaussians than the total energy. These shortcomings include that Gaussians do not properly describe Kato's cusp condition[46] and that they fade too fast at large distances, faster than required by the asymptotic conditions for the exact solutions of the Schrödinger electronic equation.

In the BO approximation, the nuclear and electronic motions are not dynamically coupled. However, as the nuclei have finite masses, it is important in very accurate calculations to account for small energy effects that are due to this coupling. Most of the adiabatic correction to the total energy of a molecular system is recovered by the DBOC. In this work, in calculating the adiabatic correction we follow the procedure described in the work of Cencek and Kutzelnigg.[47] The procedure is based on the approach proposed by Handy *et al.*,[48]

which starts with the following expression for the adiabatic correction, E_{ad}:

$$E_{ad} = -\frac{1}{2} \sum_{\alpha=1}^{K} \frac{1}{M_\alpha} \sum_{i_\alpha=1}^{3} \langle \Psi | \frac{\partial^2}{\partial Q_{i_\alpha}^2} | \Psi \rangle, \tag{5}$$

where M_α is the mass of nucleus α, Q_{i_α} is the ith coordinate of the nucleus α, and K is the number of the nuclei in the system. In Eq. (5), instead of directly differentiating the electronic wave function with respect to the nuclear coordinate Q_{i_α}, the derivative is approximated numerically as

$$\frac{\partial \Psi}{\partial Q_{i_\alpha}} \simeq \frac{\Psi\left(Q_{i_\alpha} + \frac{1}{2}\Delta Q_{i_\alpha}\right) - \Psi\left(Q_{i_\alpha} - \frac{1}{2}\Delta Q_{i_\alpha}\right)}{\Delta Q_{i_\alpha}}. \tag{6}$$

The calculation of the wave functions at a molecular geometry where the Q_{i_α} coordinate of the α nucleus was shifted by ΔQ_{i_α} (i.e., $\Psi(Q_{i_\alpha} \pm \frac{1}{2}\Delta Q_{i_\alpha})$) involves recomputation of the linear expansion coefficients through solving Eq. (4). In this work, the DBOCs have been calculated using $\Delta Q_{i_\alpha} = 5 \times 10^{-4}$ bohr. In addition, the calculation of the shifted wavefunction, $\Psi(Q_{i_\alpha} \pm \frac{1}{2}\Delta Q_{i_\alpha})$, involves adjusting the positions of the ECSGs in the basis set to the shifted position of the α nucleus. Given optimal nonlinear parameters (Gaussian exponents and centers) for the ECSG basis set at a certain nuclear configuration, $\{Q_{i_k}\}$, determined by the optimization routine, the ECSG basis set for the nuclear configuration shifted by $\frac{1}{2}\Delta Q_{i_\alpha}$ needs to be found. As the positions (and the exponential parameters $\mathbf{L}_k$) of the Gaussians are expected to change when the nuclear configuration changes, a relation needs to be found between those two changes to effectively calculate the derivative (see Eq. (6)). Unfortunately, this relation is not known in a functional form. This complicates the calculation of the DBOCs.

To evaluate the derivatives in Eq. (6), six independent BO energy calculations per atom need to be performed at each PES grid point. If such calculations were carried out in the same way as the BO energy calculations, over 255 000 BO calculations, each involving full optimizations of $\mathbf{L}_k$'s and $\mathbf{s}_k$'s, instead of the 41 655 calculations, would be needed. This would be computationally unfeasible. Therefore, instead, along the lines of the work of Cencek *et al.*,[47] a shifting procedure was devised in this work to determine the shift of the Gaussian centers for a particular shift of the coordinates of the nuclei. Below we describe the procedure emphasizing the features which make the procedure more general in comparison to the procedure proposed by Cencek *et al.*[47]

Let us first introduce 3 three-dimensional vectors, $\mathbf{Q}_1$, $\mathbf{Q}_2$, and $\mathbf{Q}_3$, containing the coordinates of the three nuclei of H_3^+. Next, we introduce three two-electron "ionic" functions, ϕ_I, ϕ_{II}, and ϕ_{III}, that have the following shifts of the Gaussian centers:

$$\mathbf{s}_i = \begin{pmatrix} \mathbf{Q}_i \\ \mathbf{Q}_i \end{pmatrix}, \tag{7}$$

where i is equal to either 1, 2, or 3. The functions are called ionic because in Eq. (7) both Gaussian centers coincide with the position of a nucleus. With that we can approximate any basis function, ϕ_k, with a product of the three ionic functions

introduced above

$$\phi_k = \phi_I \phi_{II} \phi_{III} = \exp\left[\sum_{i=1}^{3} (-\mathbf{r}'\bar{\mathbf{A}}_i \mathbf{r} + 2\mathbf{r}\bar{\mathbf{A}}_i \mathbf{s}_i - \mathbf{s}_i'\bar{\mathbf{A}}_i \mathbf{s}_i) \right], \tag{8}$$

where $\bar{\mathbf{A}}_i$ is $\mathbf{A}_i \otimes \mathbf{I}_3$. By equating like terms in Eq. (8) one gets

$$\sum_{i=1}^{3} \bar{\mathbf{A}}_i = \bar{\mathbf{A}}_k, \tag{9}$$

$$\sum_{i=1}^{3} \bar{\mathbf{A}}_i \mathbf{s}_i = \bar{\mathbf{A}}_k \mathbf{s}_k, \tag{10}$$

$$\mathbf{s}_k' \bar{\mathbf{A}}_k \mathbf{s}_k = \sum_{i=1}^{3} \mathbf{s}_i' \bar{\mathbf{A}}_i \mathbf{s}_i, \tag{11}$$

where $\mathbf{s}_k$ is the $3n$-dimensional (i.e., six-dimensional for H_3^+) Gaussian shift vector. By assuming that $\bar{\mathbf{A}}_i = a_i \bar{\mathbf{A}}_k$, Eqs. (9) and (10) become

$$\sum_{i=1}^{3} a_i = 1, \tag{12}$$

$$\sum_{i=1}^{3} a_i \mathbf{s}_i = \mathbf{s}_k. \tag{13}$$

With that Eq. (11) is automatically satisfied. Notice that Eq. (13) is actually composed of two independent equations, one for the x coordinates and one for the y coordinates. For nonlinear geometries of H_3^+, Eqs. (12) and (13) are sufficient to predict the ECSG shift vectors for the new geometrical configuration of the nuclei. The procedure involves the following steps.

1. For each ECSG construct the three auxiliary functions ϕ_{I-III} by using the H_3^+ nuclear coordinates as the shift vectors as shown in Eq. (7).
2. Solve the three independent equations, Eqs. (12) and (13), to obtain the values of the a_1, a_2, and a_3 parameters.
3. Determine the new Gaussian shift vector by inverting Eq. (13) for the new, changed H_3^+ geometry, i.e., $\mathbf{Q}_i \pm \frac{1}{2}\Delta \mathbf{Q}_i$.

However, Eqs. (12) and (13) are not independent when the H_3^+ geometry becomes linear. The linear case is dealt with by making use of those equations in Eqs. (11) and (13) which do not zero out in this situation. In addition, Eq. (11) needs to be simplified (approximated) by "decoupling" the parts corresponding to the different electrons in order to make Eqs. (9)–(11) specific to each Gaussian center. In the "decoupling" we assume that the off-diagonal terms in $\bar{\mathbf{A}}_k$ are small compared to the diagonal terms. This turns Eq. (11) into an equation that constrains the squares of the x coordinates of the Gaussian centers to the square of the corresponding x coordinate of the α nucleus

$$a_1 + a_2 + a_3 = 1, \tag{14}$$

$$a_1 x_1 + a_2 x_2 + a_3 x_3 = x_\alpha, \tag{15}$$

$$a_1 x_1^2 + a_2 x_2^2 + a_3 x_3^2 = x_\alpha^2, \tag{16}$$

where we have assumed that the linear H_3^+ lies on the x axis. With that, even for a linear H_3^+ configuration, the system of equations, Eqs. (9)–(11), is non-singular and can be solved.

III. FITTING OF THE PES

A. The grid

An appropriate choice of the grid is important for the quality of the surface fit. Traditionally, the energy is calculated at points located around the stationary points of the potential, which is a good strategy for the construction of a local, i.e., non-global, PES. The renowned PES parametrization by Meyer *et al.*,[6] the MBB surface, is based on 69 artfully selected configurations around the minimum of the potential which extend up to $25\,000$ cm^{-1}. Their parametrization has been used by others, such as Röhse *et al.*[3] or Jaquet *et al.*[49] Bachorz *et al.*[38] started from the MBB grid to which they included three additional sets of configurations. For constructing a global potential energy surface it is essential to have a grid spanning the complete configuration space. Such a grid may be constructed in a systematic manner in hyperspherical coordinates, in particular, in the so-called democratic hyperspherical coordinates.[50,51] Of these coordinates, the hyperradius, ρ, describes the overall size of the system, while the two hyperangles, θ and ϕ, describe its geometrical shape.

In the present work we have generated a very dense grid using the following ranges of the parameters and the corresponding step sizes:

$$\rho : 1 \leq \rho \leq 20, \quad \Delta\rho = 0.1,$$
$$\theta : 0° \leq \theta \leq 90°, \quad \Delta\theta = 5°, \tag{17}$$
$$\phi : 30° \leq \phi \leq 90°, \quad \Delta\phi = 5°.$$

These generate a grid consisting of 44 885 points. However, the configurations with one or more internuclear distances being smaller than $0.7\,a_0$ were eliminated leaving a total of 42 498 points. An additional 843 points were also discarded leaving a final grid of 41 655 points.[53] *Ab initio* data for these points are given in the electronic archive.[40] As can be inferred from the range of the ϕ angle, these points span only one sixth of the surface. The remaining parts of the surface were obtained by symmetry considerations. Due to the very small ρ step size, our grid is much denser than the grid used before by Viegas *et al.*,[52] which comprised 9985 points. Figure 1 illustrates the density of the grid.

B. BO surface

The three lowest singlet states of H_3^+ are intrinsically connected due to avoided crossings between the ground state and the first excited state and a conical intersection line between the first and second excited states. Viegas *et al.*,[52] who first constructed global potential energy surfaces of those three states, showed that the diatomics in molecules, DIM, approach[54] is a good starting point for an accurate description of the surfaces. In the present work we follow their approach to generate a global, high-quality potential energy surface of the electronic ground state. In the DIM approach, the PES is obtained by diagonalization of the following 3×3 matrix,

$$\mathbf{H}(\mathbf{R}) = \begin{bmatrix} E(R_1) + \epsilon(R_2, R_3) & \Delta(R_3) & \Delta(R_2) \\ \Delta(R_3) & E(R_2) + \epsilon(R_3, R_1) & \Delta(R_1) \\ \Delta(R_2) & \Delta(R_1) & E(R_3) + \epsilon(R_1, R_2) \end{bmatrix}, \tag{18}$$

where

$$E(R_i) = V_{[H_2, X^1\Sigma_g^+]}(R_i), \tag{19}$$

$$\epsilon(R_j, R_k) = \frac{1}{2}[V_{[H_2^+, X^2\Sigma_g^+]}(R_j) + V_{[H_2^+, A^2\Sigma_u^+]}(R_j) + V_{[H_2^+, X^2\Sigma_g^+]}(R_k) + V_{[H_2^+, A^2\Sigma_u^+]}(R_k)] - 2E_H, \tag{20}$$

and

$$\Delta(R_k) = \frac{1}{2}[V_{[H_2^+, X^2\Sigma_g^+]}(R_k) - V_{[H_2^+, A^2\Sigma_u^+]}(R_k)]. \tag{21}$$

In the above equations, V denotes potential energy curves of H_2 or H_2^+ and E_H is the energy of the 1s state of H, $E_H = -0.5\,E_h$, and i, j, and k are the nuclear indices. R_1 is the distance between nuclei 2 and 3, etc., and $\mathbf{R}$ is a three element vector with coordinates R_1, R_2, and R_3. In our approach we use the H_2 and H_2^+ potentials of Viegas *et al.*,[52] which are based on the accurate *ab initio* energies of Wolniewicz[55,56] ($H_2(X^1\Sigma_g^+)$), Bishop and Wetmore[57] ($H_2^+(X^2\Sigma_g^+)$), and Peek[58] ($H_2^+(A^2\Sigma_u^+)$).

The advantage of the DIM PES representation is that it correctly describes the degeneracies within the three states and within the dissociation channels. However, it is not accurate at small distances because only a limited number of the diatomic states are used and the overlap between the atomic and diatomic fragments forming H_3^+ are neglected.[54] The accuracy can be improved by adding a three-body term $V^{(3)}(\mathbf{R})$ either to the adiabatic or diabatic potential matrices.[59,60] In the latter approach, which we employ here, care is needed in order not to spoil the symmetry properties of the DIM matrix. The terms inserted to the diagonal elements of this matrix must be identical for the three matrix elements and fully symmetric with respect to the permutation of the nuclei.
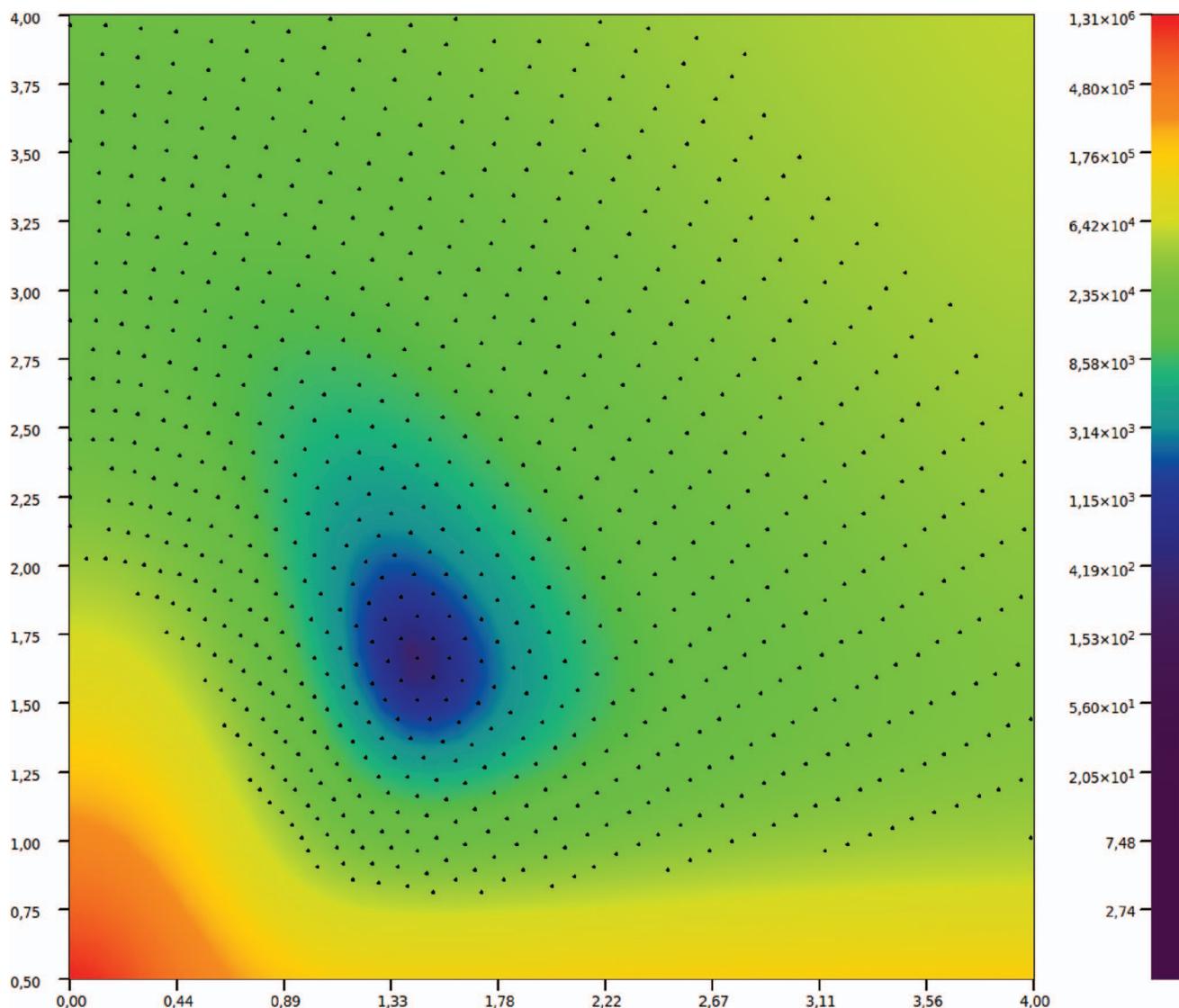
FIG. 1. Two-dimensional cut of the resulting PES as an illustration of a scope and density of a grid. The plot is in Jacobi coordinates for a fixed angle of 90°. Distances are in bohr with the horizontal axis giving the diatomic H-H distance and the vertical axis the distance of the H⁺ to diatomic center-of-mass.

Hence the diagonal matrix elements are changed to

$$H_{ii} \rightarrow H_{ii} + V^{(3)}(R_1, R_2, R_3). \qquad (22)$$

The corresponding corrections to the off-diagonal elements are

$$H_{ij} = \Delta(R_k) - \frac{1}{2}[\tilde{V}^{(3)}(R_1, R_2, R_3)]^2. \qquad (23)$$

The three-body term in Eq. (23) is squared to make the off-diagonal element, H_{ij}, negative (see Eq. (21)).

Let us now describe the functional form of the three-body terms. They are represented as polynomials of the following three functions of the standard (see Ref. 23, for example) symmetry coordinates, S_i,

$$\Gamma_1 = S_a, \quad \Gamma_2 = S_x^2 + S_y^2, \quad \Gamma_3 = S_y(S_y^2 - 3S_x^2) \quad (24)$$

known as the integrity basis functions.[61] Any product of these functions is totally symmetric with respect to permutations of the three nuclei. A detailed discussion on this point can be found in the book by Murrell *et al.*[62]

The three-body terms are then written as

$$V^{(3)}(\mathbf{R}) = P^I(\Gamma_1, \Gamma_2, \Gamma_3) T(\Gamma_1). \qquad (25)$$

They are products of polynomial P^I,

$$P^I(\Gamma_1, \Gamma_2, \Gamma_3) = \sum_{i+2j+3k \leq I} c_{ijk}\Gamma_1^i \Gamma_2^j \Gamma_3^k, \qquad (26)$$

and the following range-determining factor:

$$T(x) = [1 + e^{\gamma(x-x_0)}]^{-1}, \qquad (27)$$

which damps the three-body terms at large distances where the DIM approximation takes over. The summation in Eq. (26) includes all possible terms up to order I with respect to the symmetry coordinates S_i. The symmetry coordinates, S_i, are expressed in terms of expansion coordinates $\tilde{R}_i$ (see Viegas *et al.*[52] for details), for which we use, following Meyer *et al.*,[6] the Morse displacement coordinates

$$\tilde{R}_i = [1 - e^{-\beta_\alpha(R_i/R_{0,\alpha}-1)}]/\beta_\alpha. \qquad (28)$$

TABLE I. Parameters of expansion functions: for the two three-body terms, the order of the polynomial and the resulting number of linear coefficients is given together with the numerical values of the nonlinear parameters.

Term	Order	#Coef	γ	R_0	β	x_0
Diagonal	15	174	0.3	2.50	1.0	10.0
Off-diagonal	13	123	0.3	2.50	1.0	12.0

The analytical expression for the potential energy surface contains linear expansion parameters c_{ijk} of the three-body terms and nonlinear parameters of the range-determining factors and the Morse expansion functions. The initial values of the nonlinear parameters were taken from our previous fit[52] and the linear parameters were determined by least-squares fitting. Next, the nonlinear parameters were adjusted manually by a trial-and-error procedure. A summary of the procedure is given in Table I. The *ab initio* data points used to generate the fit describe the energy region up to 6000 cm^{-1} above the dissociation limit. A few configurations have been omitted as they were found to spoil the overall quality of the fit. These were asymptotic configurations for which at least two internuclear distances are bigger than 9.0 a$_0$. Such configurations are well described by the DIM approach without the three body corrections (i.e., by the pure DIM representation). In the FORTRAN code, where the PES fit is calculated, the representation of the potential that includes the three-body terms is automatically replaced by the pure DIM representation for asymptotic configurations.

The quality of the fit generated in this work can be evaluated based on Fig. 2, which shows the deviation between calculated points and their representation by the fit. Two further figures are given in the electronic archive[40] which give two-dimensional cuts through the full PES. For most configurations, the fit switches correctly to the asymptotic pure DIM representation. Unphysical behavior is observed for a few configurations located well above the fitted energy range. This range would require a description in terms of three electronic states, which we will attempt in future work.

The overall root mean square, rms = $(\sum_1^N (V(i) - E(i))^2/N)^{\frac{1}{2}}$, for the PES representation obtained from N = 7840 points with 297 parameters in the fitting function is rms = 0.097 cm^{-1}. As mentioned, the 7840 points span only one sixth of the whole PES, the complete surface is obtained based on 47 040 points. Of the calculated points not used in generating the fit most correspond to configurations with high energies. These points will be needed in our future work concerning the H$_3^+$ metastable states located above the dissociation threshold.

An important aspect of this fit is the very large number of *ab initio* points used, which allows the PES to be fully determined at all geometries within the region of interest, and its correct representation at linear geometries. Both these issues have been discussed in Ref. 63.

C. Correction surfaces

The DBOC points are fitted not globally, but only up to 30 000 cm^{-1} as here we only consider nuclear motion up to this energy. The fit to the symmetric corrections was performed using polynomials in terms of symmetry coordinates[23] S_a, S_x, and S_y. Ninety-eight parameters were fitted to about 4000 points giving an analytic surface which reproduced the points with a standard deviation of 0.007 cm^{-1}. For the mixed isotopologues, the DBOC obeys special
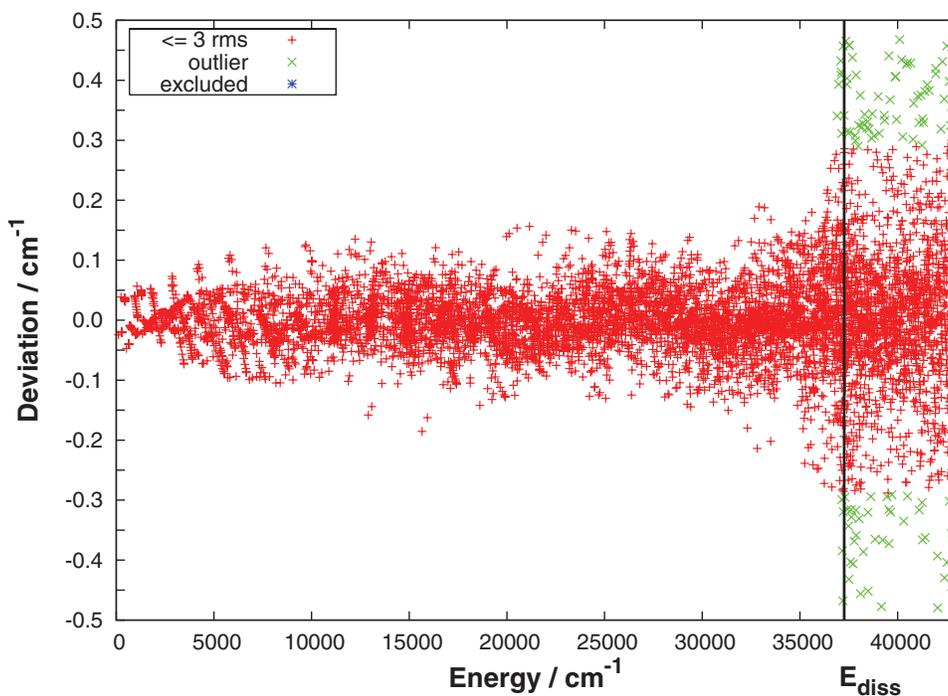
FIG. 2. An illustration of the quality of the analytical fit of the ground-state H$_3^+$ PES: residuals for the *ab initio* grid points used in the fit as function of their energy above the PES minimum. The vertical line marks the dissociation energy.
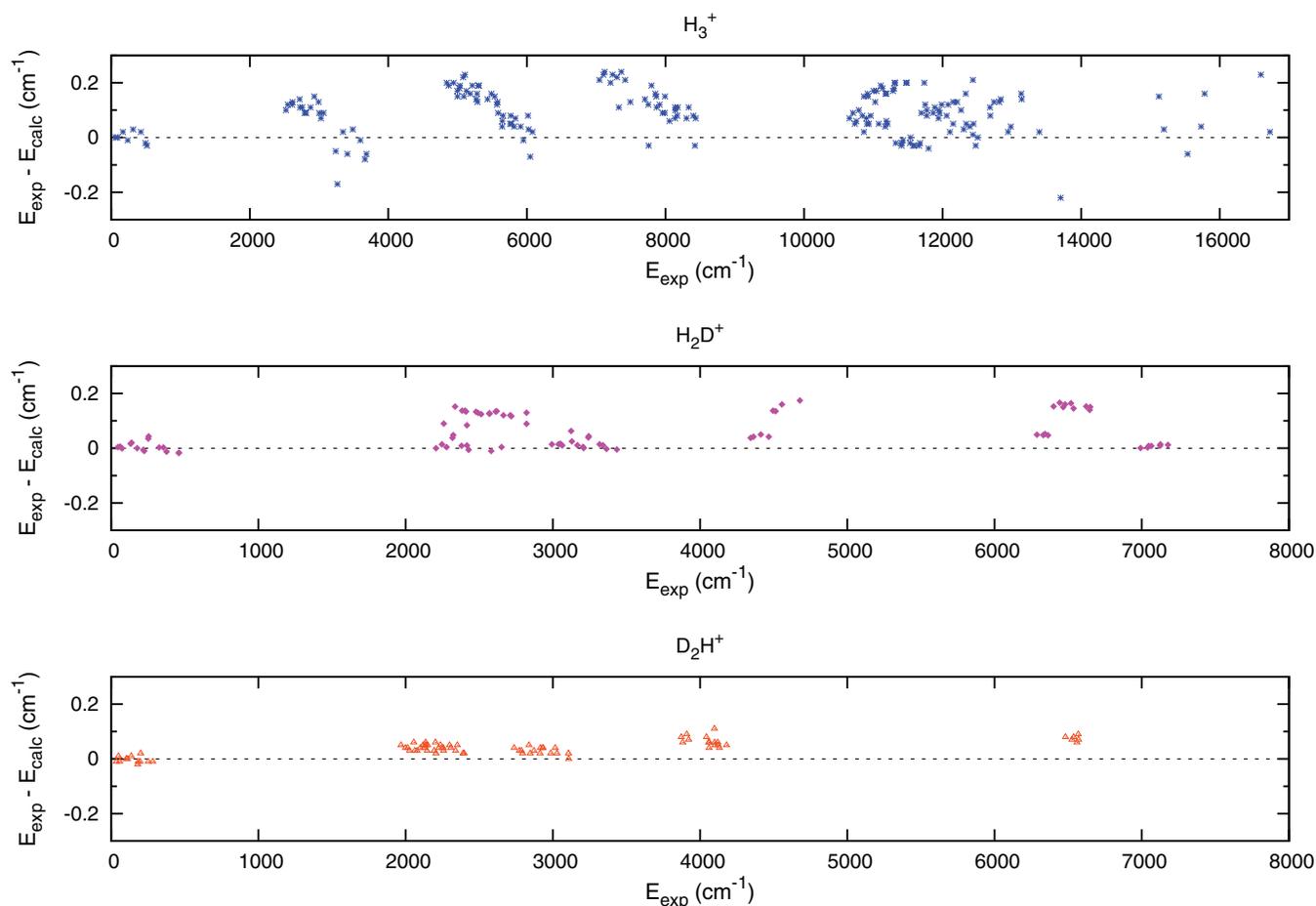
FIG. 3.   Residuals (observed minus calculated) for all observed states with $J = 0, 1, 2, 3$ for H_3^+, H_2D^+, and D_2H^+. Calculations are performed with the GLH3P potential, the non-adiabatic model,[23] and DVR3D.

symmetry rules[64] and an extra surface was fitted using a standard functional form.[23]

The data for the relativistic correction were taken from the work of Bachorz *et al.*[38] and fitted up to $30\,000$ cm^{-1} using an analytical surface with six constants[23] and a standard deviation of 0.007 cm^{-1}. This surface was then added to the symmetric DBOC. These fits are given in the electronic archive.[40] We call our final PES, including the correction surfaces, GLH3P.

IV. NUCLEAR MOTION COMPUTATIONS

We used the GLH3P PES in calculations of ro-vibrational energy levels. Calculations considering both rotational and vibrational motion were performed up to $17\,000$ cm^{-1}, the region covered by available experimental studies, and for $J = 0$ up to $25\,000$ cm^{-1}, to the end of the visible region. The calculations used the BO surface as well as relativistic and adiabatic corrections, as well as non-adiabatic corrections which are discussed below. The studies considered H_3^+, H_2D^+, and D_2H^+. We do not consider D_3^+ here as experimental data are only available for the bending fundamental.

To make direct comparisons with the extensive results available from high-resolution molecular spectroscopy for H_3^+ (Refs. 8–11, and 13) and the mixed isotopologues H_2D^+ and

D_2H^+,[14–21] a series of variational rotation-vibration computations were performed using the adiabatic PESs of this study and exact kinetic energy operators. These computations utilized the DVR3D program suite[65] and previously tested basis sets, the D^{2}FOPI code[66–68] with appropriate basis sets to deal with singularities present in the ro-vibrational Hamiltonian,[68] and the Hyperspherical harmonics code.[69, 70]

Both DVR3D and D^{2}FOPI have been adapted to allow for both vibrational and rotational non-adiabatic effects.[71] Initially, all nuclear motion calculations used nuclear masses, the preferred choice when mass-dependent adiabatic surfaces are available. The variational procedures employed, without the non-adiabatic corrections, give energies which agree within 0.01 cm^{-1}, in line with previous[72] comparisons. In contrast to the electronic structure calculations, all nuclear-motion calculations presented here were performed on desktop computers.

The numerical calculations with the hyperspherical harmonics code of Wolniewicz proceed in two steps: First, for each value of the angular momentum, J, and each symmetry, Γ, the corresponding hyperspherical harmonics are generated and the potential matrix is set up in this basis, for each hyperradial grid point. In the present work, we calculate the matrix at 300 points within $0.5\,a_0 \leq \rho \leq 6.0\,a_0$. In Wolniewicz's algorithm,[69] the size of the hyperspherical harmonic expansion is controlled by a single input parameter, $K_{\max}$, which

TABLE II. Difference between observed[11] and calculated line frequencies for higher J states of H_3^+. Three lines are reassigned; for these the final column gives the obs.−calc. difference for the previous assignment, which is also given.

Line	Band (v_1, v_2, l)	Obs. cm^{-1}	Calc. cm^{-1}	Obs.−Calc. cm^{-1}	o.− c., old assig. cm^{-1}
tP(3, 0)	(2,2,2)	10322.235	10322.211	0.02	
R(6, 6)	Unknown	10329.307			
nR(2, 2)	(0,4,4)	10366.546	10366.433	0.11	
nR(2, 1)	(0,4,4)	10367.184	10367.038	0.15	
nR(3, 3)	(0,4,4)	10454.539	10454.394	0.15	
P(6, 6)	Unknown	10462.405	10462.493	− 0.09	
tQ(2, 1)	(2,2,2)	10467.800	10467.701	0.10	
tQ(3, 1)	(2,2,2)	10468.544	10468.442	0.10	
R(5, 5)	Unknown	10496.287	10496.122	0.17	
nP(2, 1)	(2,2,2)	10496.571	10496.562	0.01	
tR(4, 4)	(2,2,2)	10497.078	10496.886	0.19	
nP(3, 2)	(2,2,2)	10507.396	10507.406	− 0.01	
P(4, 3)	(2,2,2)	10528.992	10529.038	− 0.05	
nP(5, 5)l	(2,2,2)	10558.882	10559.012	− 0.13	
tQ(3, 0)	(2,2,2)	10560.443	10560.363	0.08	
tQ(1, 0)	(2,2,2)	10568.209	10568.131	0.08	
R(4, 3)	Unknown	10573.997	10573.837	0.16	
nP(1, 1)	(2,2,2)	10581.256	10581.218	0.04	
nP(3, 3)	(2,2,2)	10583.688	10583.719	− 0.03	
nP(2, 2)	(2,2,2)	10586.424	10586.424	0.00	
tR(3, 3)	(2,2,2)	10609.077	10608.913	0.16	
tR(2, 2)	(2,2,2)	10621.634	10621.479	0.16	
P(4, 3)	(0,5,1)	10624.888	10624.814	0.07	
P(4, 4)	(0,5,1)	10632.042	10632.078	− 0.04	
Q(5, 0)	Unknown	10639.058	10638.824	0.23	
tR(1, 1)	(2,2,2)	10641.024	10640.897	0.13	
+6Q(3, 0)	(0,5,3)	10657.149	10656.968	0.18	
Q(5, 3)	Unknown	10666.604	10666.415	0.19	
nQ(1, 1)	(2,2,2)	10669.815	10669.754	0.06	
nQ(2, 1)	(2,2,2)	10671.864	10671.801	0.06	
nP(4, 4)u	(2,2,2)	10686.611	10686.622	− 0.01	
tR(4, 3)	(2,2,2)	10690.240	10690.062	0.18	
tR(3, 2)	(2,2,2)	10705.364	10704.971	0.39[a]	
P(3, 2)	(0,5,1)	10705.894	10705.756	0.14	
Q(4, 3)u	(0,5,1)	10710.311	10710.128	0.18	
tR(2, 1)	(2,2,2)	10725.953	10725.807	0.15	
P(3, 3)	(0,5,1)	10730.107	10730.035	0.07	
tR(1, 0)	(2,2,2)	10752.150	10752.042	0.11	
P(2, 2)	(0,5,1)	10752.369	10752.278	0.09	
nQ(3, 2)u	(2,2,2)	10760.627	10760.490	0.14	
nQ(2, 2)	(2,2,2)	10766.108	10766.070	0.04	
P(2, 1)	(0,5,1)	10766.320	10766.182	0.14	
Q(3, 2)u	(0,5,1)	10779.136	10779.092	0.04	
+6Q(2, 1)	(0,5,3)	10789.844	10789.709	0.13	
nQ(4, 2)u	(2,2,2)	10793.060	10793.021	0.04	
P(3, 0)	(0,5,1)	10798.691	10798.490	0.20	
P(1, 1)	(0,5,1)	10798.785	10798.652	0.13	
+6Q(3, 1)	(0,5,3)	10803.820	10803.595	0.23	
tR(3, 1)	(2,2,2)	10805.800	10805.622	0.18	
P(5, 3)l	(0,5,1)	10811.027	10810.882	0.15	
P(3, 1)u	(0,5,1)	10813.699	10813.528	0.17	
+6Q(4, 1)	(0,5,3)	10816.758	10816.537	0.22	
Q(1, 0)	(0,5,1)	10831.677	10831.526	0.15	
nR(1, 1)	(2,2,2)	10845.089	10844.994	0.09	
nQ(4, 3)	(2,2,2)	10847.551	10847.629	− 0.08	
Q(4, 2)u	(0,5,1)	10855.172	10854.962	0.21	

TABLE II. (*Continued.*)

Line	Band (v_1, v_2, l)	Obs. cm^{-1}	Calc. cm^{-1}	Obs.−Calc. cm^{-1}	o.− c., old assig. cm^{-1}
P(6, 6)	(3,1,1)	10874.681	10875.095	− 0.41	
nR(2, 1)	(2,2,2)	10934.327	10934.204	0.12	
tR(3, 0)	(2,2,2)	10935.358	10935.113	0.25	−0.12 Q(3, 0)
Q(3, 0)	(0,5,1)	10935.631	10935.477	0.15	0.52 tR(3, 0)
Q(1, 1)	(0,5,1)	10939.559	10939.374	0.18	
P(5, 5)	(3,1,1)	10953.026	10953.644	− 0.62[a]	
+6R(1, 1)	(0,5,3)	10963.072	10962.870	0.20	
Q(2, 2)	(0,5,1)	10964.605	10964.418	0.19	
+6R(2, 2)	(0,5,1)	10964.792	10964.574	0.22	
Q(3, 3)	(0,5,1)	10968.257	10968.110	0.15	
P(4, 3)	(3,1,1)	11015.488	11015.619	− 0.13	
nR(2, 2)u	(2,2,2)	11019.351	11019.157	0.19	
nR(3, 1)u	(2,2,2)	11024.705	11025.223	− 0.52[a]	
P(4, 4)	(3,1,1)	11033.268	11033.421	− 0.15	
R(6, 6)	Unknown	11036.111			
R(1, 1)l	(0,5,1)	11044.146	11043.931	0.22	
R(5, 5)	Unknown	11046.569	11046.415	0.15	
R(4, 4)	Unknown	11048.996	11048.794	0.20	
R(3, 3)u	(0,5,1)	11053.686	11053.424	0.26	
Q(2, 1)u	(0,5,1)	11071.117	11070.892	0.23	
P(3, 3)	(3,1,1)	11111.798	11111.726	0.07	
nR(4, 3)	(2,2,0)	11114.428	11114.293	0.14	
R(5, 0)	Unknown	11114.628	11114.454	0.17	
R(3, 2)u	(0,5,1)	11195.630	11195.343	0.28	
R(1, 0)	(0,5,1)	11228.601	11228.321	0.28	
R(1, 1)u	(0,5,1)	11244.353	11244.085	0.27	
R(2, 1)l	(0,5,1)	11246.707	11246.405	0.30	
Q(3, 0)	(3,1,1)	11278.517	11278.537	− 0.02	
R(2, 2)l	(0,5,1)	11304.480	11304.199	0.28	
Q(1, 0)	(3,1,1)	11318.080	11318.099	− 0.02	
P(6, 6)	Unknown	11331.112	11331.214	− 0.10	
Q(3, 3)	(3,1,1)	11358.855	11358.915	− 0.06	
−6P(5, 5)u	(0,5,1)	11422.627	11422.689	− 0.06	
−6P(4, 4)	(0,5,3)	11482.938	11482.967	− 0.03	
P(4, 3)	(0,5,5)	11494.835	11494.892	− 0.06	−1.33 P(3,3)
R(4, 3)	Unknown	12331.180	12330.898	0.28	
tQ(1, 0)	(0,6,2)	12419.140	12419.124	0.02	
P(3, 3)	(0,6,2)	12502.614	12502.659	− 0.05	
tQ(3, 3)	(1,4,4)	12525.302	12525.250	0.05	
R(3, 0)	Unknown	12536.621	12536.423	0.20	
tQ(1, 1)	(1,4,4)	12623.171	12623.057	0.11	
nR(3, 3)	(1,4,2)	12658.335	12658.114	0.22	
tR(1, 0)	(1,4,4)	12897.888	12897.786	0.10	
R(1, 0)	(0,6,2)	13056.013	13055.763	0.25	
Q(1, 0)	(0,6,4)	13597.367	13597.389	− 0.02	
R(3, 3)	Unknown	13606.093	13605.820	0.27	
Q(1, 0)	(0,7,1)	13676.446	13676.197	0.25	
R(2, 0)	hot	10827.764	10827.500	0.26	
R(2, 3)	hot	11265.189			

[a]Probable misassigned line.

is the maximum value of the grand angular momentum. We have used here $K_{max} = 140$, which, for $J = 0$, yields 444 functions of symmetry A_1', 408 functions of symmetry A_2', and 852 functions of symmetry E'. The basis has then been contracted to a convenient size N as described by Wolniewicz and Hinze.[70] The ro-vibrational eigenvalues are obtained in the second step, where a system of N coupled equations in the hyperradius, ρ, is integrated numerically using the matrix Numerov algorithm with a step size of $\Delta\rho = 0.01 \, a_0$ and an interval $0.5 \, a_0 \leq \rho \leq 6.0 \, a_0$. The potential matrices are interpolated by cubic splines. Numerical tests were made to guarantee the convergence of the eigenvalues with respect to boundaries of the integration interval and the step size. More critical is the number of coupled equations, N. While $N = 100$

is appropriate for the lowest eigenvalues (up to 10 000 cm^{-1}), it has to be increased for the higher ones. We made numerical tests with N up to $N = 250$. For the calculations in symmetry E', $N = 200$ was found to give fully converged results for eigenvalues up to 30 000 cm^{-1}. Note that there are 129 eigenvalues up to this energy. The calculations in symmetries A_1' and A_2' can be done with less coupled equations, as the density of states is lower (86 and 45 states, respectively). $N = 150$ was found to be sufficient. Our reported eigenvalues are converged with respect to all these parameters to $10^{-9} E_h$.

The CPU time on a single processor (Intel Xenon X5650) is about 12 min for the preparation of the potential matrices, step 1, and roughly 30 s per eigenvalue with $N = 100$, 100 s with $N = 150$, 250 s with $N = 200$ and 400 s with $N = 250$ in step 2. The precise CPU time depends on the density of states and time needed to find upper and lower bounds for each eigenvalue.

Calculations of ro-vibrational energies up to 30 000 cm^{-1} (25 000 cm^{-1} when allowance is made for the zero-point energy) were performed with and without non-adiabatic corrections. First, the BO surface plus adiabatic corrections was used. The discrepancy between theory and experiment proved to be within 2 cm^{-1} for observed transition frequencies up to 13 000 cm^{-1} .[9–12] As all the parts of the calculations are performed with an accuracy of approaching 0.01 cm^{-1}, the only possible source of this discrepancy could be non-adiabatic effects. We therefore used a simple method to allow for non-adiabatic correction as developed in Ref. 23: the kinetic energy (KE) operator was modified by using different vibrational and rotational masses. The vibrational mass was taken as intermediate between nuclear and atomic, and equal to 1.007 537 u, a value taken from studies of H_2^+ by Moss.[73] For the deuterated species we also employed the formula of Moss, see Ref. 23 for details. The rotational mass was taken to be equal to the nuclear mass. As only J up to 3 was considered, we did not have to modify the rotational mass as for low J rotational non-adiabatic effects are negligible. The difference in the two masses leads to an additional kinetic energy operator term[23] which is zero when the two masses are equal.

Table III gives results of these calculations for transitions observed in the visible. After re-assigning four previously misassigned transitions, the maximum deviation is about 0.2 cm^{-1} and the standard deviation is less than 0.1 cm^{-1}. Detailed comparison with the newly observed transitions in the mid-visible region were given in Ref. 13 and are of similar quality.

The real test of any beyond-Born–Oppenheimer model is that it should be capable of giving results of similar quality for all isopotologues of a system. In this context the asymmetric isotopologues, H_2D^+ and D_2H^+, provide a particularly stringent test since an accurate calculation of the splitting of the degenerate H_3^+ ν_2 bending mode upon asymmetric isotopic substitution requires non-Born–Oppenheimer terms of a lower symmetry than the BO PES.[74,75] The results of the calculations for energy levels up to $J = 3$ for H_3^+, H_2D^+, and D_2H^+ are given in the electronic archive.[40] For H_2D^+ and D_2H^+ we undertook a systematic check on the labelling of the energy levels using the rigid rotor decomposition procedure.[76]

TABLE III. Selected calculated transition frequencies of H_3^+ in cm^{-1}. Column I-rotational assignment, II-observed line center,[10,12] III-calculated frequency using the model of Ref. 23, IV-observed – calculated in this model, V-observed – calculated using a nuclear mass model. Note the four reassigned lines.

I	IIs	III	IV	V
Q(1,0)	10831.681	10831.520	0.16	− 0.80
P(1,1)	10798.777	10798.650	0.13	− 0.84
R(1,0)[a]	10752.161	10752.040	0.12	− 1.04
R(2,2)[b]	10752.161	10755.590		− 3.55
P(1,1)	12413.247	12413.280	0.03	− 1.17
R(1,1)	12588.951	12588.910	0.04	− 1.28
R(1,1)	12620.223	12620.080	0.14	− 1.10
Q(1,1)	12373.526	12373.270	0.26	− 1.05
R(1,1)	12381.137	12381.070	0.07	− 1.06
R(1,1)	12678.688	12678.520	0.17	− 1.06
R(1,1)[a]	13332.903	13332.850	0.05	− 1.32
P(1,1)[b]	13332.903	13332.393		0.51
Q(1,0)	13638.251	13638.430	0.18	− 1.31
P(1,1)	15058.681	15058.490	0.19	− 1.25
P(1,1)	15130.480	15130.430	0.05	− 1.34
R(1,0)	15450.112	15450.190	0.08	− 1.54
R(1,0)	15643.052	15643.000	0.05	− 1.44
Q(1,1)	15716.813	15716.590	0.22	− 1.34
R(1,0)[a]	16506.139	16505.920	0.21	− 1.38
P(1,0)[b]	16506.139	16495.969		− 10.17
Q(1,0)[a]	16660.216	16660.210	0.00	− 1.55
P(1,0)[b]	16660.216	16670.796		− 10.58

[a]New assignment on the basis of the calculations presented here.
[b]Previous assignment.

These largely confirmed the previous labels, even in cases where these were not particularly secure.[21]

A summary of differences between the published observed and calculated levels with $J = 0$, 1, 2, and 3 is presented in Fig. 3. As seen from the figure, the results for all isotopologues are of similar high quality. All, however, show a small, systematic shift which places the calculated levels slightly too low. This discrepancy could be easily decreased further by slight reduction in the effective vibrational mass reducing the maximum deviation to about 0.1 cm^{-1} and a standard deviation of about 0.05 cm^{-1}. However, this would destroy the purely *ab initio* character of this model and was not pursued here. A further reduction in this discrepancy would require more sophisticated modeling of non-adiabatic effects; we return to this point below.

Tables II and III compare our *ab initio* calculations with observations for various high-lying states of H_3^+. Not only are our new calculations significantly better than previous studies but also we are able to make (re-)assignments for a number of lines which have previously proved problematic. For example, the transition at 13 676 cm^{-1} was reproduced so badly, a discrepancy of over 3 cm^{-1}, by the previous calculations that Bachorz *et al.*[38] concluded that the reason of such discrepancy was not yet known. Our calculations reproduce this line with an accuracy similar to the others. As indicated in the table, there are three lines which are probably misassigned. To confirm this will require further calculations with higher J levels; this will form part of a future study.

TABLE IV. $J = 0$ vibrational band origins calculated using the hyperspherical method in full symmetry.

v_1	v_2	ℓ	Γ	n	E/cm^{-1}
0	0	0	A_1'	0	0.00
0	1	1	E'	0	2521.30
1	0	0	A_1'	1	3178.29
0	2	0	A_1'	2	4778.15
0	2	2	E'	1	4997.89
1	1	1	E'	2	5554.20
2	0	0	A_1'	3	6262.13
0	3	1	E'	3	7005.97
0	3	3	A_1'	4	7285.56
0	3	3	A_2'	0	7492.78
1	2	0	A_1'	5	7769.23
1	2	2	E'	4	7870.23
2	1	1	E'	5	8488.01
0	4	0	A_1'	6	9001.57
0	4	2	E'	6	9113.04
3	0	0	A_1'	7	9251.91
1	3	1	E'	7	9653.70
1	3	3	A_1'	8	9968.94
0	4	4	E'	8	9997.18
1	3	3	A_2'	1	10210.33
2	2	0	A_1'	9	10593.19
2	2	2	E'	9	10645.31
0	5	1	E'	10	10862.75
0	5	3	A_1'	10	10923.36
3	1	1	E'	11	11323.12
0	5	3	A_2'	2	11529.24
0	5	5	E'	12	11658.31
1	4	0	A_1'	11	11814.52
1	4	2	E'	13	12079.40
4	0	0	A_1'	12	12146.46
2	3	1	E'	14	12303.33
0	6	0	A_1'	13	12382.15
0	6	2	E'	15	12477.39
2	3	3	A_1'	14	12590.53
1	4	4	E'	16	12697.40
2	3	3	A_2'	3	12832.17
3	2	0	A_1'	15	13288.91
3	2	2	E'	17	13318.19
1	5	1	E'	18	13395.20
1	5	3	A_1'	16	13405.25
0	6	4	E'	19	13592.25
0	7	1	E'	20	13702.58
0	7	3	A_1'	17	13725.43
1	5	3	A_2'	4	13756.61
4	1	1	E'	21	14055.01
2	4	0	A_1'	18	14198.51
1	5	5	E'	22	14218.02
2	4	2	E'	23	14478.22
0	7	3	A_2'	5	14566.28
1	6	0	A_1'	19	14666.18
1	6	2	E'	24	14890.47
3	3	1	E'	25	14901.82
0	8	0	A_1'	20	14909.87
5	0	0	A_1'	21	14940.15
0	6	6	A_1'	22	15080.18
0	8	2	E'	26	15122.64
3	3	3	A_1'	23	15168.30
0	6	6	A_2'	6	15190.71
2	4	4	E'	27	15214.80

TABLE IV. (*Continued.*)

v_1	v_2	ℓ	Γ	n	E/cm^{-1}
1	6	4	E'	28	15335.96
3	3	3	A_2'	7	15373.68
2	5	1	E'	29	15791.11
4	2	0	A_1'	24	15877.85
4	2	2	E'	30	15888.28
2	5	3	A_1'	25	15925.04
2	5	3	A_2'	8	15969.60

Finally, Table IV gives our predicted vibrational band origins for H_3^+ for states up to $16\,000$ cm^{-1}; a full list of the 263 band origins we predict to lie below $25\,000$ cm^{-1} is given in the electronic archive.[40] The results presented were obtained with using the Hyperspherical harmonics code since this works in full symmetry but are closely mirrored by calculations performed using the programs D^{2}FOPI and DVR3D. Vibrational assignments have been included where possible; however, H_3^+ is well known to show very strong couplings leading to an early onset of classical chaos and a loss of approximate vibrational quantum numbers.[77] These predicted band origins provide a starting point for further, higher frequency experimental studies.

V. SUMMARY AND CONCLUSIONS

We present a highly accurate global PES of H_3^+ molecular ion, which resulted from extra high accuracy non-relativistic electronic structure BO calculation in a grid of 41 655 points which give high density coverage of all H_3^+ geometries up to and well above dissociation and global fit of these *ab initio* points using three PESs of interacting electronic states. Adiabatic corrections to the BO approximation have also been computed.

We used three independent nuclear motion codes to calculate rotation-vibration lines to compare our calculated line centers to experimentally known ones. We have done it both without and with modeling of non-adiabatic effects. Lines known experimentally are both below and above the barrier to linearity. The calculated discrepancy between theory and experiment proved to be better than 0.1 cm^{-1} on average, once both adiabatic and non-adiabatic corrections to the Born–Oppenheimer approximation are explicitly included in the calculation. We are confident that the presented results will allow us to predict accurately the rotation-vibration levels of H_3^+ in vicinity of dissociation and assist the experimental observation of the lines close to dissociation.

Overall, for the ground-state PES of H_3^+ and its isotopologues, the largest remaining source of error in the prediction of ro-vibrational transition frequencies lies in the treatment of non-adiabatic effects and, possibly, inclusion of effects due to quantum electrodynamics.[86]

The present work uses the Polyansky–Tennyson[23] approach of a fixed, effective vibrational mass to represent non-adiabatic effects. Furthermore, this treatment includes no allowance for rotational non-adiabatic effects which will result in it becoming increasingly less accurate with

rotational excitation, *J*. It is well known from studies on diatomic systems that non-adiabatic effects are geometry dependent and, therefore, high-accuracy treatments require the use of coordinate dependent masses.[78,79] Bunker and Moss[80] formulated a method for treating non-adiabatic effects in triatomic molecules but so far studies that have considered non-adiabatic effects in triatomic systems have been very limited.[81–84] For example, an empirically motivated approach due to Schiffels *et al.*[82] introduces energy-dependent corrections to the band origins. Recently, *ab initio* methods for calculating effective, coordinate-dependent rotational and vibrational masses have been proposed.[79,85] A logical follow-up to the present study is to implement such an approach for the H_3^+ system.

In short, this paper presents (a) an extremely accurate global potential energy surface of H_3^+ resulting from high accuracy *ab initio* calculations and a global fit, (b) very accurate calculations for all available experimental energy levels up to $16\,000$ cm^{-1} above the ground state, (c) results that suggest we can predict accurately the lines of H_3^+ towards dissociation and thus facilitate their experimental observation.

ACKNOWLEDGMENTS

[1]S. Bubin, M. Cafiero, and L. Adamowicz, Adv. Chem. Phys. **131**, 377 (2005).

[2]G. C. Lie and D. Frye, J. Chem. Phys. **96**, 6784 (1992).

[3]R. Röhse, W. Kutzelnigg, R. Jaquet, and W. Klopper, J. Chem. Phys. **101**, 2231 (1994).

[4]O. L. Polyansky, R. Prosmiti, W. Klopper, and J. Tennyson, Mol. Phys. **98**, 261 (2000).

[5]M. Pavanello, W.-C. Tung, F. Leonarski, and L. Adamowicz, J. Chem. Phys. **130**, 074105 (2009).

[6]W. Meyer, P. Botschwina, and P. Burton, J. Chem. Phys. **84**, 891 (1986).

[7]I. R. McNab, Adv. Chem. Phys. **89**, 1 (1995).

[8]C. M. Lindsay and B. J. McCall, J. Mol. Spectrosc. **210**, 60 (2001).

[9]J. Gottfried, B. McCall, and T. Oka, J. Chem. Phys. **118**, 10890 (2003).

[10]H. Kreckel, D. Bing, S. Reinhardt, A. Petrignani, M. Berg, and A. Wolf, J. Chem. Phys. **129**, 164312 (2008).

[11]C. P. Morong, J. L. Gottfried, and T. Oka, J. Mol. Spectrosc. **255**, 13 (2009).

[12]M. Berg, Ph.D. dissertation, University of Heidelberg, 2010.

[13]M. Pavanello, L. Adamowicz, A. Alijah, N. F. Zobov, I. I. Mizus, O. L. Polyansky, J. Tennyson, T. Szidarovszky, A. G. Császár, M. Berg, A. Petrignani, and A. Wolf, Phys. Rev. Lett. **108**, 023002 (2012).

[14]T. Amano and J. K. G. Watson, J. Chem. Phys. **81**, 2869 (1984).

[15]T. Amano, J. Opt. Soc. Am. B **2**, 790 (1985).

[16]S. C. Foster, A. R. W. McKellar, I. R. Peterkin, J. K. G. Watson, and F. S. Pan, J. Chem. Phys. **84**, 91 (1986).

[17]S. C. Foster, A. R. W. McKellar, and J. K. G. Watson, J. Chem. Phys. **85**, 664 (1986).

[18]O. L. Polyansky and A. R. W. McKellar, J. Chem. Phys. **92**, 4039 (1989).

[19]M. Farnick, S. Davis, M. A. K. O. L. Polyansky, J. Tennyson, and D. J. Nesbitt, J. Chem. Phys. **116**, 6146 (2002).

[20]P. Hlavenka, R. Plasil, G. Bano, I. Korolov, J. Ramanlal, J. Tennyson, J. Glosik, and D. Gerlich, Int. J. Mass Spectrom. **255–256**, 170 (2006).

[21]O. Asvany, E. Hugo, S. Schlemmer, F. Muller, F. Kuhnemann, S. Schiller, and J. Tennyson, J. Chem. Phys. **127**, 154317 (2007).

[22]T. Yonezu, F. Matsushima, Y. Moriwaki, K. Takagi, and T. Amano, J. Mol. Spectrosc. **256**, 238 (2009).

[23]O. L. Polyansky and J. Tennyson, J. Chem. Phys. **110**, 5056 (1999).

[24]K. Chakrabarti and J. Tennyson, Euro. J. Phys. D **66**, 31 (2012).

[25]T. P. Snow and B. J. McCall, Annu. Rev. Astron. Astrophys. **44**, 367 (2006).

[26]S. Miller, N. Achilleos, G. E. Ballester, T. R. Geballe, R. D. Joseph, R. Prange, D. Rego, T. Stallard, J. Tennyson, L. M. Trafton, and J. H. Waite, Jr., Philos. Trans. R. Soc. London, Ser. A **358**, 2485 (2000).

[27]T. T. Koskinen, A. D. Aylward, and S. Miller, Nature (London) **450**, 845 (2007).

[28]S. Miller, J. Tennyson, S. Lepp, and A. Dalgarno, Nature (London) **355**, 420 (1992).

[29]P. Drossart, J. P. Maillard, J. Caldwell, S. J. Kim, J. K. G. Watson, W. A. Majewski, J. Tennyson, S. Miller, S. Atreya, J. Clarke, J. H. Waite, Jr., and R. Wagener, Nature (London) **340**, 539 (1989).

[30]L. Kao, T. Oka, S. Miller, and J. Tennyson, Astrophys. J. Suppl. **77**, 317 (1991).

[31]L. Neale, S. Miller, and J. Tennyson, Astrophys. J. **464**, 516 (1996).

[32]T. Sochi and J. Tennyson, Mon. Not. R. Astron. Soc. **405**, 2345 (2010).

[33]L. Neale and J. Tennyson, Astrophys. J. **454**, L169 (1995).

[34]S. Miller, T. Stallard, H. Melin, and J. Tennyson, Faraday Discuss. **147**, 283 (2010).

[35]C. M. Coppola, L. Lodi, and J. Tennyson, Mon. Not. R. Astron. Soc. **415**, 487 (2011).

[36]A. Carrington, I. R. McNab, and Y. D. West, J. Chem. Phys. **98**, 1073 (1992).

[37]W. Cencek, J. Rychlewski, R. Jaquet, and W. Kutzelnigg, J. Chem. Phys. **108**, 2831 (1998).

[38]R. A. Bachorz, W. Cencek, R. Jaquet, and J. Komasa, J. Chem. Phys. **131**, 024105 (2009).

[39]M. Pavanello and L. Adamowicz, J. Chem. Phys. **130**, 034104 (2009).

[40]See supplementary material at http://dx.doi.org/10.1063/1.4711756 for electronic versions of all the the potential energy surfaces as FORTRAN programs plus numerical values of the electronic and vibration-rotation energies.

[41]S. G. Nash, SIAM (Soc. Ind. Appl. Math.) J. Numer. Anal. **21**, 770 (1984).

[42]M. Pavanello, W. C. Tung, and L. Adamowicz, Phys. Rev. A **81**, 042526 (2010).

[43]W. Cencek, J. Komasa, and J. Rychlewski, Chem. Phys. Lett. **246**, 417 (1995).

[44]J. Komasa, Mol. Phys. **104**, 2193 (2006).

[45]W. Cencek, J. Komasa, K. Pachucki, and K. Szalewicz, Phys. Rev. Lett. **95**, 233004 (2005).

[46]T. Kato, Commun. Pure Appl. Math. **10**, 151 (1957).

[47]W. Cencek and W. Kutzelnigg, Chem. Phys. Lett. **266**, 383 (1997).

[48]N. C. Handy, Y. Yamaguchi, and H. F. Schaefer III, J. Chem. Phys. **84**, 4481 (1986).

[49]R. Jaquet, W. Cencek, W. Kutzelnigg, and J. Rychlewski, J. Chem. Phys. **108**, 2837 (1998).

[50]R. C. Whitten and F. T. Smith, J. Math. Phys. **9**, 1103 (1968).

[51]B. R. Johnson, J. Chem. Phys. **73**, 5051 (1980).

[52]L. P. Viegas, A. Alijah, and A. J. C. Varandas, J. Chem. Phys. **126**, 074309 (2007).

[53]The exclusion of the 843 geometry points was due to a technicality: A glitch in the FORTRAN code employed for the conversion to Cartesian coordinates, needed by the ECG code, generated inaccurate coordinates for these points. The remaining 41 655 points have been double-checked afterwards and the accuracy of their coordinates confirmed.

[54]F. O. Ellison, J. Am. Chem. Soc. **85**, 3540 (1963).

[55]L. Wolniewicz, J. Chem. Phys. **99**, 1851 (1993).

[56]L. Wolniewicz, J. Chem. Phys. **103**, 1792 (1995).

[57]D. M. Bishop and R. W. Wetmore, Mol. Phys. **26**, 145 (1973).

[58] J. M. Peek, J. Chem. Phys. **43**, 3004 (1965).

[59] I. Last and M. Baer, J. Chem. Phys. **75**, 288 (1981).

[60] A. J. C. Varandas and A. I. Voronin, Mol. Phys. **95**, 497 (1995).

[61] H. Weyl, *The Classical Theory of Groups* (Princeton University, 1946).

[62] J. N. Murrell, S. Carter, S. C. Farantos, P. Huxley, and A. J. C. Varandas, *Molecular Potential Energy Functions* (Wiley, Chichester, 1984).

[63] O. L. Polyansky, A. Alijah, N. F. Zobov, I. I. Mizus, R. Ovsyannikov, J. Tennyson, L. Lodi, T. Szidarovszky, and A. G. Császár, "Spectroscopy of H_3^+ based on new high accuracy global potential energy surface," Philos. Trans. R Soc. London, Ser. A (in press).

[64] O. L. Polyansky, B. M. Dinelli, C. R. Le Sueur, and J. Tennyson, J. Chem. Phys. **102**, 9322 (1995).

[65] J. Tennyson, M. A. Kostin, P. Barletta, G. J. Harris, O. L. Polyansky, J. Ramanlal, and N. F. Zobov, Comput. Phys. Commun. **163**, 85 (2004).

[66] G. Czakó, T. Furtenbacher, A. G. Császár, and V. Szalay, Mol. Phys. **102**, 2411 (2004).

[67] T. Furtenbacher, G. Czakó, B. T. Sutcliffe, A. G. Császár, and V. Szalay, J. Mol. Struct. **780–781**, 283 (2006).

[68] T. Szidarovszky, G. Czakó, and A. G. Császár, Phys. Chem. Chem. Phys. **12**, 8373 (2010).

[69] L. Wolniewicz, J. Chem. Phys. **90**, 371 (1989).

[70] L. Wolniewicz and J. Hinze, J. Chem. Phys. **101**, 9817 (1994).

[71] J. Tennyson, P. Barletta, M. A. Kostin, O. L. Polyansky, and N. F. Zobov, Spectrochim. Acta, Part A **58**, 663 (2002).

[72] O. L. Polyansky, A. G. Császár, S. V. Shirin, N. F. Zobov, P. Barletta, J. Tennyson, D. W. Schwenke, and P. J. Knowles, Science **299**, 539 (2003).

[73] R. E. Moss, Mol. Phys. **89**, 195 (1999).

[74] W. J. Briels, J. Tennyson, M. Claessens, T. van der Lee, and A. van der Avoird, Int. J. Quantum Chem. **23**, 1091 (1983).

[75] B. M. Dinelli, O. L. Polyansky, and J. Tennyson, J. Chem. Phys. **103**, 10433 (1995).

[76] E. Mátyus, C. Fábri, T. Szidarovszky, G. Czakó, W. D. Allen, and A. G. Császár, J. Chem. Phys. **133**, 034113 (2010).

[77] J. Tennyson, Rep. Prog. Phys. **57**, 421 (1995).

[78] C. Schwartz and R. J. Le Roy, J. Mol. Spectrosc. **121**, 420 (1987).

[79] R. Jaquet and W. Kutzelnigg, Chem. Phys. **346**, 69 (2008).

[80] P. R. Bunker and R. E. Moss, J. Mol. Spectrosc. **80**, 217 (1980).

[81] D. W. Schwenke, J. Phys. Chem. A **105**, 2352 (2001).

[82] P. Schiffels, A. Alijah, and J. Hinze, Mol. Phys. **101**, 175 (2003).

[83] P. Schiffels, A. Alijah, and J. Hinze, Mol. Phys. **101**, 189 (2003).

[84] A. Alijah, J. Mol. Spectrosc. **264**(2), 111 (2010).

[85] K. Pachucki and J. Komasa, J. Chem. Phys. **130**, 164113 (2009).

[86] P. Pyykko, K. G. Dyall, A. G. Csaszar, G. Tarczay, O. L. Polyansky, and J. Tennyson, Phys. Rev. A **63**, 024502 (2001).